Inorg. Chem. **2006**, *45*, 7698–7704

Ferromagnetic Exchange Interactions for Cu_6^{12+} and Mn_6^{12+} Hexagons Sandwiched by Two B-α-$[XW_9O_{33}]^{9-}$ (X = As^{III} and Sb^{III}) Ligands in D_{3d}-Symmetric Polyoxotungstates

Toshihiro Yamase,*,† Keisuke Fukaya,† Hiroyuki Nojiri,‡ and Yuhgo Ohshima‡

Chemical Resources Laboratory, Tokyo Institute of Technology, R1-21 4259 Nagatsuta, Midori-ku, Yokohama 226-8503, Japan, "Creation of bio-devices and bio-systems with chemical and biological molecules for medical use", CREST, Japan Science and Technology Agency, and Institute for Material Research, Tohoku University, 2-1-1 Katahira, Aoba-ku, Sendai 980-8577, Japan

Received April 19, 2006

Two novel Cu_6 and Mn_6 hexagon sandwiched polyoxometalates, $[(CuCl)_6(AsW_9O_{33})_2]^{12-}$ (**1a**) and $[(MnCl)_6(SbW_9O_{33})_2]^{12-}$ (**2a**), have been synthesized and characterized by X-ray single-crystal analysis and magnetic measurements. These complexes are D_{3d} symmetric and were isolated as $[n\text{-}BuNH_3]^+$ salts from aqueous solutions: $(n\text{-}BuNH_3)_{12}[(CuCl)_6(AsW_9O_{33})_2]\cdot 6H_2O$ (**1**), rhombohedral, $R\bar{3}$, a = 20.33(1) Å, c = 26.35(2) Å, Z = 3 and $(n\text{-}BuNH_3)_{12}[(MnCl)_6(SbW_9O_{33})_2]\cdot 6H_2O$ (**2**). Six Cu (or Mn) atoms, each of which shows 5-fold coordination, make an approximately equatorial hexagon with a first-neighboring Cu···Cu (Mn···Mn) distance of 2.913(2) Å (3.248(1) Å) and a Cu–O–Cu (Mn–O–Mn) bond angle of 94.5(2)° (100.4(2)°). The magnetic behavior investigated by magnetic susceptibility measurements shows the ferromagnetic exchange interactions with J/k = +12.7 K (J/hc = +8.82 cm^{-1}) and a S = 3 ground state for **1** and J/k = +0.20 K (J/hc = +0.14 cm^{-1}) and a S = 15 ground state for **2**, when only J refers to the isotropic magnetic-exchange interactions for first-neighbor atoms of the approximately equilateral Cu_6^{12+} and Mn_6^{12+} hexagons. The single-crystal ESR spectroscopy of **1** under the orientation of the magnetic field along a Cu_6 hexagon's nearly 6-fold axis equal to the c axis on the variation of temperature supports the S = 3 ground state and allows an estimate of the zero-field (fine-structure) energy separation between S_z = 0 and S_z = ±1 of D = –0.182 K to be obtained.

Introduction

Much attention has been paid to magnetically significant polyoxometalates for the development of nanoscale molecular magnets.[1] The magnetic behavior of a variety of such polyoxometalates has been explored during the past decade with the aim of designing single molecular magnets.[2] Recently, we have shown that the spin-frustrated $(VO)_3^{6+}$ triangle for $[(VO)_3(SbW_9O_{33})_2]^{12-}$ and $[(VO)_3(BiW_9O_{33})_2]^{12-}$ is a good model of the magnetization (associated with two doublets with a different spin chirality) between pure quantum states S = 1/2 and 3/2 and provides a new class of single-molecule magnets,[3] as well as a new class of antiviral

* To whom correspondence should be addressed: E-mail: tyamase@res.titech.ac.jp. Telefax: +81-45-924-5260.

† Tokyo Institute of Technology and CREST, Japan Science and Technology Agency.

‡ Tohoku University.

(1) (a) Müller, A.; Peter, F.; Pope, M. T.; Gatteshi, D. *Chem. Rev.* **1998**, *98*, 239. (b) Coronado, E.; Gómez-Garcia, C. J. *Chem. Rev.* **1998**, *98*, 273. (c) Clemente-Juan, J. M.; Coronado, E. *Coord. Chem. Rev.* **1999**, *193*−*195*, 361. (d) Mialane, P.; Dolbecq, A.; Marrot, J.; Rivière, E.; Sécheresse, F. *Chem.*−*Eur. J.* **2005**, *11*, 1771. (f) Schröder, C.; Nojiri, H.; Schnack, J.; Hage, P.; Luban, M.; Kögerler, P. *Phys. Rev. Lett.* **2005**, *94*, 172505. (g) Bi, L.; Kortz, U.; Nellutia, S.; Stowe, A. C.; van Tol, J.; Dalal, N. S.; Keita, B.; Nadjo, L. *Inorg. Chem.* **2005**, *44*, 896.

(2) (a) Clemente-Juan, J. M.; Andres, H.; Borrás-Almenar, J. J.; Coronado, E.; Güdel, H.-U.; Aebersold, M.; Kearly, G.; Büttner, H.; Zelliker, M. *J. Am. Chem. Soc.* **1999**, *121*, 10021. (b) Andres, H.; Clemente-Juan, J. M.; Aebersold, M.; Güdel, H.-U.; Coronado, E.; Büttner, H.; Kearly, G.; Melero, J.; Burriel, R. *J. Am. Chem. Soc.* **1999**, *121*, 10028. (c) Clemente-Juan, J. M.; Coronado, E.; Gaita-Ariño, A.; Giménez-Saiz, C.; Chaboussant, G.; Güdel, H.-U.; Burriel, R.; Mutka, H. *Chem.*−*Eur. J.* **2002**, *8*, 5701. (d) Kortz, U.; Nellutla, S.; Stowe, A. C.; Dalal, N. S.; van Tod, J.; Bassil, B. S. *Inorg. Chem.* **2004**, *43*, 144. (e) Stowe, A. C.; Nellutla, S.; Dalal, N. S.; Kortz, U. *Eur. J. Inorg. Chem.* **2004**, 3792. (f) Clemente-Juan, J. M.; Coronado, E.; Gaita-Ariño, A.; Giménez-Saiz, C.; Güdel, H.-U.; Sieber, A.; Bircher, R.; Mutka, H. *Inorg. Chem.* **2005**, *44*, 3389.

(3) Yamase, T.; Ishikawa, E.; Fukaya, K.; Nojiri, H.; Taniguchi, T.; Atake, T. *Inorg. Chem.* **2004**, *43*, 8150.

10.1021/ic060666f CCC: $33.50 © 2006 American Chemical Society
Published on Web 08/23/2006

polyoxometalates against a wide variety of enveloped RNA viruses.[4] The observation of a half-step quantum magnetization resulting from the antisymmetrical Dzyaloshinsky−Moriya interaction for the spin-frustrated triangle-spin ring has been done by the use of single crystals of $Na_{12}[\{Cu(H_2O)\}_3(AsW_9O_{33})_2]\cdot 32H_2O$.[5] The structure of $[(VO)_3(XW_9O_{33})_2]^{12-}$ (X = Sb^{III} and Bi^{III}) for the spin-frustrated $(VO)_3^{6+}$-triangle polyoxometalates consists of a VO^{2+} (with a square-pyramidal 5-fold coordination V^{4+} center) triangle cluster, sandwiched by two diamagnetic α-B-$[XW_9O_{33}]^{9-}$ (X = Sb^{III} and Bi^{III}) ligands in D_{3h} local symmetry. In our continuing investigation of a molecular design of simple single-molecule magnets based on polyoxometalates, we found the ferromagnetic behavior of 5-fold coordination Cu_6^{12+} and Mn_6^{12+} hexagons for $[(CuCl)_6(AsW_9O_{33})_2]^{12-}$, $[(CuBr)_6(AsW_9O_{33})_2]^{12-}$, $[(CuCl)_6(SbW_9O_{33})_2]^{12-}$, and $[(MnCl)_6(SbW_9O_{33})_2]^{12-}$ with D_{3d} symmetry for each. Such a 5-fold coordination transition-metal-ion hexagon sandwiched by two α-B-$[XW_9O_{33}]^{9-}$ ligands is structurally different from the Sn_6^{12+} hexagon consisting of three 4- and three 6-fold coordinated Sn^{2+} ions in D_{3h}-symmetrical $[Sn_6(SnW_9O_{33})_2]^{8-}$.[6] The D_{3d}-symmetric polyoxotungstates containing Cu_6^{12+} and Mn_6^{12+} hexagons provides a simple model for the exchange-interaction study of molecular magnets, as expected in the preparation of the 6-fold coordinated Cu_4^{8+} center-incorporated polyoxometalates for a better understanding of the magnetic behavior.[2d,2e] Although the ferromagnetic Cu_6^{12+}-hexagon compound, as a molecular magnetic material, was at first reported with $[(PhSiO_2)_6Cu_6(O_2SiPh)_6]\cdot 6EtOH$ as one of the Cu^{2+}-containing polyorganosiloxanato clusters,[7] there has been no example for the Cu_6^{12+}-hexagon polyoxometalates. As ferromagnetic polyoxometalates, so far, 6-fold coordination transition-metal clusters, such as $[Ni_4(H_2O)_2(P_2W_{15}O_{56})_2]^{16-}$,[8] $[M_4(H_2O)_2(PW_9O_{34})_2]^{10-}$ (M=Co^{II}, Ni^{II}),[2a,2b] $[Co_3W_4(D_2O)_2(ZnW_9O_{34})_2]^{12-}$,[2c] $[Ni_3Na(H_2O)_2(XW_9O_{34})_2]^{11-}$ (X=P^V, As^V),[9,10] $[Ni_6(H_2O)_2(AsW_9O_{34})_2(AsW_6O_{26})]^{17-}$,[10] $[Ni_4Mn_2(H_2O)_2(PW_9O_{34})_2(PW_6O_{26})]^{17-}$,[10] $[\{\gamma\text{-}SiW_{10}O_{36}Cu_2(H_2O)(N_3)_2\}_2]^{12-}$, and $[\{\gamma\text{-}SiW_8O_{31}Cu_3(OH)(H_2O)(N_3)\}_3(N_3)]^{19-}$, have been recognized, and the two isolated $[Cu_2(\mu_{1,1}-N_3)_2]$ pairs in $[\{\gamma\text{-}SiW_{10}O_{36}Cu_2(H_2O)(N_3)_2\}_2]^{12-}$ have been estimated to be most strongly ferromagnetically coupled with $J/hc = +224$ cm^{-1}.[1d] We describe herein the synthesis and the structural characterization of $(n\text{-}BuNH_3)_{12}[(CuCl)_6(AsW_9O_{33})_2]\cdot 6H_2O$ (**1**) and $(n\text{-}BuNH_3)_{12}[(MnCl)_6(SbW_9O_{33})_2]\cdot 6H_2O$ (**2**) and discuss the ferromagnetic properties of 5-fold coordination Cu_6^{12+} and Mn_6^{12+} hexagons.

Experimental Section

Synthesis. $(n\text{-}BuNH_3)_{12}[(CuCl)_6(AsW_9O_{33})_2]\cdot 6H_2O$ (**1**) was prepared by replacement of a lanthanides moiety of $(n\text{-}BuNH_3)_{12}[\{Eu(H_2O)\}_2(AsW_9O_{33})_2]\cdot 8H_2O$ with a Cu_6 hexagon. After filtration of an aqueous solution containing $(n\text{-}BuNH_3)_{12}[\{Eu(H_2O)\}_2(AsW_9O_{33})_2]\cdot 8H_2O$ (0.6 g, 0.1 mmol) and $CuCl_2$ (1.0 g, 7.4 mmol) in 30 mL, the filtrate was kept for approximately one month at room temperature, and orange crystals (0.18 g in 29% based on W) were isolated. Anal. Calcd: C, 9.44; H, 2.57; N, 2.75; Cu, 6.24; W, 54.19; As, 2.45; Cl, 3.48%. Found: C, 9.33; H, 2.36; N, 2.81; Cu, 6.2; W, 54.3; As, 2.6; Cl, 3.64%. IR (KBr disk): showed metal−oxygen stretches $\bar{\nu}$ = 948 (m), 901 (m), 870 (m), 836 (s), 810 (m), 763 (s), 733 (s), 699 (s) cm^{-1}.

$(n\text{-}BuNH_3)_{12}[\{Eu(H_2O)\}_2(AsW_9O_{33})_2]\cdot 8H_2O$ was prepared as follows.[11] An aqueous solution (10 mL) of $Eu(NO_3)_3\cdot 6H_2O$ (0.23 g, 0.5 mmol) was added into an aqueous solution (40 mL) of $Na_9[AsW_9O_{33}]\cdot 19.5H_2O$[12] (1.4 g, 0.5 mmol) and warmed to approximately 80 °C. *n*-$BuNH_3Cl$ (0.55 g, 5 mmol, solid) was added to the warm solution, and the resulting solution was kept at room temperature for a few days to yield colorless crystals (0.73 g, 49% based on W) of $(n\text{-}BuNH_3)_{12}[\{Eu(H_2O)\}_2(AsW_9O_{33})_2]\cdot 8H_2O$. Anal. Calcd for $C_{48}N_{12}H_{168}O_{78}As_2Eu_2W_{18}$: C, 9.73; N, 2.84; H, 2.86; Eu, 5.13; W, 55.85; As, 2.53%. Found: C, 9.64; N, 2.91; H, 2.52; Eu, 5.1; W, 56.0; As, 2.6%. IR (KBr disk): metal−oxygen stretches $\bar{\nu}$ = 939 (m), 857 (s), 778 (s), 727 (s) cm^{-1}. The preparation of **1** from the reaction of $Na_9[AsW_9O_{33}]\cdot 19.5H_2O$ (0.56 g, 0.2 mmol), $CuCl_2$, and *n*-$BuNH_3Cl$ failed.

$(n\text{-}BuNH_3)_{12}[(MnCl)_6(SbW_9O_{33})_2]\cdot 6H_2O$ (**2**) was prepared as follows. After filtration of an aqueous solution containing $Na_9[SbW_9O_{33}]\cdot 19.5H_2O$[13] (0.57 g, 0.2 mmol), $MnCl_2\cdot 4H_2O$ (1.5 g, 7.5 mmol), and *n*-$BuNH_3Cl$ (0.55 g, 5 mmol) in 30 mL, the filtrate was kept approximately for one week at room temperature, and brown crystals (0.35 g in 57% based on W) were isolated. Anal. Calcd: C, 9.38; H, 2.56; N, 2.73; Mn, 5.36; W, 53.82; Sb, 3.96; Cl, 3.46%. Found: C, 9.39; H, 2.23; N, 2.80; Mn, 5.6; W, 53.7; Sb, 4.0; Cl, 3.34%. IR (KBr disk): 942 (m), 899 (m), 854 (m), 813 (s), 725 (s), 683 (m) cm^{-1}.

$Na_9[AsW_9O_{33}]\cdot 19.5H_2O$[12] and $Na_9[SbW_9O_{33}]\cdot 19.5H_2O$[13] were synthesized by literature procedures. All chemicals were of at least analytical grade and used without further purification.

X-ray Crystallography. Intensity data for the single-crystal X-ray crystallography of **1** and **2** were measured on a Rigaku RAXIS−RAPID imaging plate diffractometer with a graphite-monochromated Mo Kα (λ = 0.71069 Å) radiation at −100 °C. Lorentz polarization effects and numerical absorption corrections (the programs Numabs and Shape; Higashi, T. *Program for Absorption Correction*; Rigaku Corporation: Tokyo, 1999) were applied to the intensity data, and H atoms were not indicated in the calculation. All the atoms (except for disordered atoms) were refined anisotropically, and the disordered atoms were refined isotropically. All the calculations were performed using the CrystalStructure software package (*CrystalStructure 3.5.1*: *Crystal*

(4) Yamase, T. *J. Mater. Chem.* **2005**, *45*, 4773.
(5) Choi, K.-Y.; Matsuda, Y.; Nojiri, H.; Kortz, U.; Hussain, F.; Stowe, A. C.; Ramsey, C.; Dalal, N. S. *Phys. Rev. Lett.* **2006**, *96*, 107202.
(6) Sokrova, M. N.; Izarolov, N. V.; Virovets, A. V.; Fedin, V. P.; Starikova, Z. A.; Yu Antipin, M. *Dalton Trans.* **2003**, 4389.
(7) (a) Ruiz, E.; Cano, J.; Alvarez, S.; Caneschi, A.; Gatteschi, D. *J. Am. Chem. Soc.* **2003**, *125*, 6791. (b) Rentschler, E.; Gatteschi, D.; Cornia, A.; Fabretti, A. C.; Barra, A.-L.; Shchegolikhina, O. I.; Zhdanov, A. A. *Inorg. Chem.* **1996**, *35*, 4427.
(8) Gómez-Garcí, C. J.; Borrás-Almenar, J. J.; Coronado, E.; Ouahab, L. *Inorg. Chem.* **1994**, *33*, 4016.
(9) Kortz, U.; Mbomekalle, I. M.; Keita, B.; Nadjo, L.; Berthet, P. *Inorg. Chem.* **2002**, *41*, 6412.
(10) Mbomekalle, I. M.; Keita, B.; Nierlich, M.; Kortz, U.; Berthet, P.; Nadjo, L. *Inorg. Chem.* **2003**, *42*, 5143.
(11) Single-crystal X-ray crystallography of $(n\text{-}BuNH_3)_{12}[\{Eu(H_2O)\}_2(AsW_9O_{33})_2]\cdot 8H_2O$ indicates a = 11.853(6) Å, b = 16.07(1) Å, c = 18.27(1) Å, α = 64.10(2)°, β = 85.83(2)°, γ = 87.81(3)°, Z = 1, V = 9614(16) $Å^3$, ρ = 3.14 g cm^{-3}, and space group $P\bar{1}$ (No. 2). The structure solved by a direct method of SHELXS86 together with the luminescence property of the peculiar Eu^{3+} site of 7-fold coordination will be shown in another paper.
(12) Tourné, C.; Revel, A.; Tourné, G.; Vendrell, M. *C. R. Acad. Soc. Paris, Ser. C* 1973, *t277*, 643. IR (KBr disk): 931 (m), 903 (s), 781 (s), 725 cm^{-1} (s).
(13) Bösing, M.; Loose, L.; Pohlman, H.; Krebs, B. *Chem.−Eur. J.* **1997**, *3*, 1232. IR (KBr disk): 925 (m), 891 (s), 769 (s), 708 cm^{-1} (s).

Structure Analysis Package; Rigaku and Rigaku/MSC: Tokyo, 2000−2003).[14]

For **1**, 31 078 reflections (ω scan and $2\theta_{max} = 54.9°$) were collected, of which 4796 unique reflections ($R_{int} = 0.054$) were used. Crystal data: MW = 6106.93, space group = $R\bar{3}$ (No. 148), $a = 20.33(1)$ Å, $c = 26.35(2)$ Å, $Z = 3$, V = 9431(9) Å^3, $\rho = 3.23$ g cm^{-3}, $\mu = 181.37$ cm^{-1}, $F(000) = 8334$, crystal size = 0.40 × 0.38 × 0.23 mm, transmission factors = 0.02−1.00. The structure was solved by a direct method (SHELXS-97) and refined based on 4313 observed reflections with $I > 2\sigma(I)$ and 245 parameters to $R_1 = 0.026$ and $R_w = 0.083$ (refined against $|F^2|$). The highest residual electron density was 1.22 e Å^{-3}. The site occupancies of four C (C5, C6, C9, and C10) atoms were fixed at 1/2. Thus, **1** was formulated as $(C_4H_9NH_3)_{12}[(CuCl)_6(AsW_9O_{33})_2]\cdot 6H_2O$.

For **2**, 31 682 reflections (ω scan and $2\theta_{max} = 55.0°$) were collected, of which 4917 unique reflections ($R_{int} = 0.060$) were used. Crystal data: MW = 6148.94, space group = $R\bar{3}$ (No. 148), $a = 20.15(1)$ Å, $c = 27.36(2)$ Å, $Z = 3$, $V = 9624(9)$ Å^3, $\rho = 3.18$ g cm^{-3}, $\mu = 172.7$ cm^{-1}, $F(000) = 8370$, crystal size = 0.30 × 0.25 × 0.05 mm, transmission factors = 0.03−0.42. The structure was solved by a direct method (SHELXS-97) and refined based on 4916 observed reflections (all with $I > 0.0\sigma(I)$) and 245 parameters to $R_1 = 0.022$ (refined against $|F|$) for $I > 2\sigma(I)$ and $R_w = 0.073$ (refined against $|F^2|$) for $I > 0.0\sigma(I)$. The highest residual electron density was 1.39 e Å^{-3}. The site occupancies of the C5, C6, C9, and C10 atoms were fixed at 1/2.

Instrumentation, Magnetic Measurements, and ESR. IR spectra were recorded on Jasco FT-IR 5000 spectrometer. The contents of As, Sb, Cu, Mn, and W were determined by X-ray fluorescence analysis (with an accuracy of 2% with a fundamental parameter method for the pellet of sample) on a Shimadzu EDX-800 spectrometer. The water content was measured by thermogravimetric methods on an ULVAC-TGD9600MTS9000 instrument. The magnetic susceptibility in the range of 1.8−300 K was measured with a Quantum Design MPMS-XL5 SQUID magnetometer, and the experimental data were corrected for the diamagnetic contribution using standard Pascal constants.[15] X-band ESR measurements were carried out on a JEOL ESR spectrometer (JES−RE1X). ESR measurements (190 GHz) were done on a homemade spectrometer at the Institute for Material Research, Tohoku University, Japan.

Results and Discussion

Structures. Figure 1a shows the structure of anion **1a** for the compound **1** which can be described as a dimer of $[(CuCl)_3(AsW_9O_{33})]^{6-}$ building blocks related by an inversion center with a resultant D_{3d} symmetry. Each building block is formed by a diamagnetic B-α-$[AsW_9O_{33}]^{9-}$ polyanion coordinated to the $(CuCl)^+-Cu^{II}$ ion triangle (with Cu···Cu = 5.045(2) Å and 60° = Cu···Cu···Cu), which corresponds to the moiety removing the $[AsW_9O_{33}]^{9-}$ ligand from the hypothetical D_{3h}-symmetrical $[(CuCl)_3(AsW_9O_{33})_2]^{15-}$ with the same geometry as the above $[(VO)_3(SbW_9O_{33})_2]^{12-}$ [16a] and $[(VO)_3(BiW_9O_{33})_2]^{12-}$ [16b] and also $[(VO)_3(AsW_9O_{33})_2]^{11-}$,[16c] $[Cu_3(H_2O)_2(AsW_9O_{33}$ or $SbW_9O_{33})_2]^{12-}$,[16d] $[\{Cu(H_2O)\}_3(AsW_9O_{33}$ or $SbW_9O_{33})_2]^{12-}$,[16e] $[\{Mn(H_2O)\}_3(AsW_9O_{33})_2]^{12-}$,[16f] $[\{Mn(H_2O)\}_3(SbW_9O_{33})_2]^{12-}$,[16g] and $[(PhSn)_3(SbW_9O_{33})_2]^{9-}$.[16h]

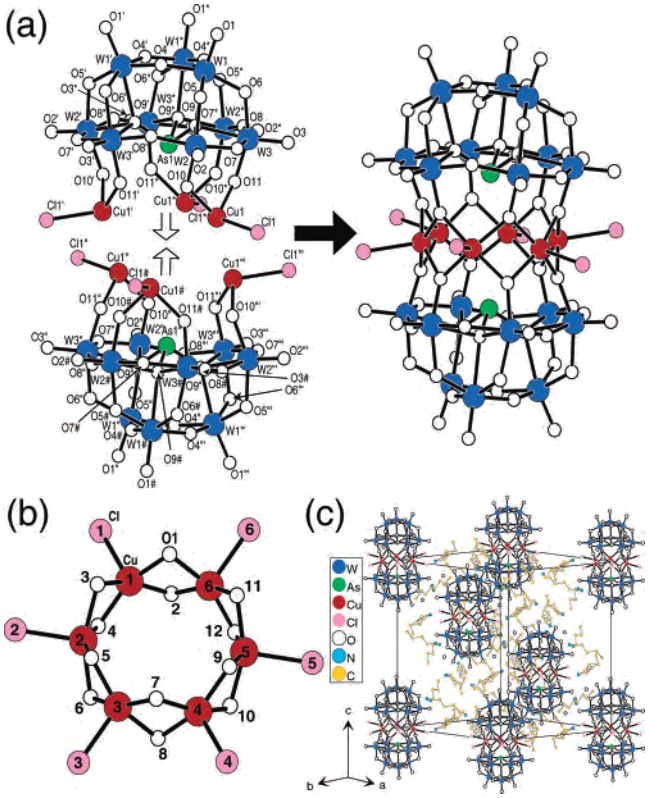

Figure 1. Formation and structure (a) of $[(CuCl)_6(AsW_9O_{33})_2]^{12-}$ (**1a**), equilateral Cu_6^{12+} hexagon and numbering scheme (b) for **1a**, and crystal packing (c) of $(n\text{-}BuNH_3)_{12}[(CuCl)_6(AsW_9O_{33})_2]\cdot 6H_2O$ (**1**): green = As, red = Cu, yellow = C, blue = N, dark blue = W, pink = Cl, and white = O.

Figure 1b and c shows the structure of the Cu_6-hexagon moiety and the packing of the molecules in the unit cell, respectively. The Cu atom for **1a** is coordinated by four oxygen atoms (with Cu−O distances of 1.968(7)−1.991(6) Å) belonging to two B-α-$[AsW_9O_{33}]^{9-}$ ligands and an exterior Cl atom (with a Cu−Cl distance of 2.490(3) Å) in a square pyramidal geometry and is on average 0.40(1) Å above the four-oxygen-atom plane. Six Cu atoms make an approximately equatorial hexagon (with a first-neighbor Cu···Cu distance of 2.913(2) Å, a Cu−O−Cu bond angle of 95.3(2)°, neighboring Cu−Cu−Cu angles of 119.98(6)°, and second- and third-neighbor Cu···Cu distances of 5.045(2) and 5.825(1) Å). The anion charges are neutralized by twelve *n*-butylammonium cations around the anion. The least-squares plane of the Cu_6^{12+} hexagon is positioned at a symmetrical distance from the two As atoms with an As···As distance of 5.278(2) Å along the *c* axis in the unit cell. The shortest Cu···Cu distance between neighboring anions is 11.076(1) Å.

Compound **2** shows the same space group and geometry as **1**. However, the substitution of Cu^{2+} by Mn^{2+} in the anion results in slightly larger Mn−O−Mn bond angle of 99.8(2)° and a lengthening of the Mn−O bond distances of 2.101(4)−2.126(4) Å and first-, second-, and third-neighbor Mn···Mn distances of 3.248(2), 5.625(1), and 6.495(2) Å for the equatorial Mn_6^{12+} hexagon because of the replacement of As^{III} (As−O bond distance of 1.784(6) Å for the trigonal pyramidal AsO_3) with Sb^{III} (Sb−O bond distance of 1.964(5)

(14) Further details on the crystal structure investigations are given in CIF files as Supporting Information.
(15) O'Conner, C. J. *Prog. Inorg. Chem.* **1982**, *29*, 203.

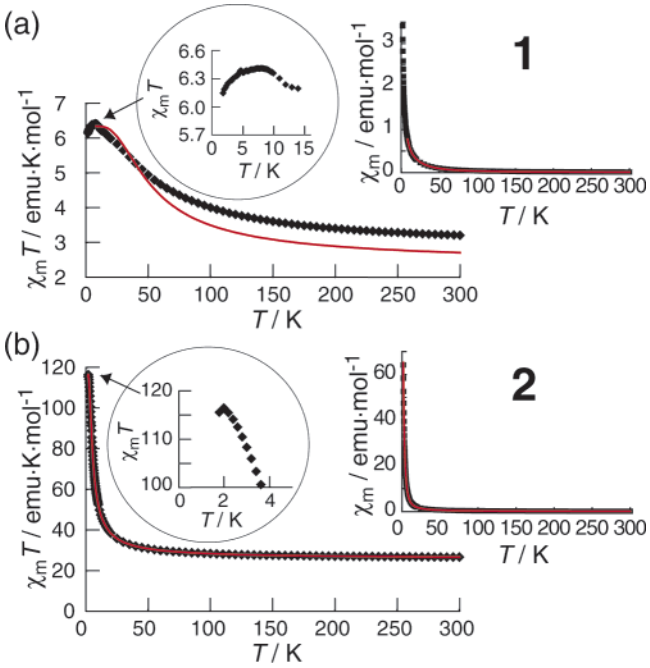

Figure 2. Temperature dependences of χ_m and $\chi_m T$ for $(n\text{-BuNH}_3)_{12}$-$[(CuCl)_6(AsW_9O_{33})_2]\cdot 6H_2O$ (**1**) and $(n\text{-BuNH}_3)_{12}[(MnCl)_6(SbW_9O_{33})_2]\cdot 6H_2O$ (**2**) at 0.10 and 0.05 T, respectively. Red lines represent the calculated curves of χ_m vs T and $\chi_m T$ vs T curves above the cusp temperature using the best-fitting parameters (in the text).

Å) which has a larger ionic radius and which showed an expectedly shorter Sb···Sb distance of 4.943(1) Å in the anion framework.[16]

Magnetic Properties. The molar magnetic susceptibility (χ_m) and its temperature product ($\chi_m T$) versus T plots for polycrystalline samples under a magnetic field (0.10 and 0.05 T for **1** and **2**, respectively) are shown in Figure 2. Values of $\chi_m T$ for **1** (or **2**) increase upon cooling from 3.2 (27.0) emu K mol^{-1} at 300 K, which corresponds to the sums of spin-only contributions (2.3 emu K mol^{-1} for 6 Cu^{2+} and 26.3 emu K mol^{-1} for 6 Mn^{2+}), and reach a maximum of 6.4 (118) emu K mol^{-1} around 7(2) K and decreases to 6.0 (70) emu K mol^{-1} at around 0 K. The behavior of the $\chi_m T$ against T plots for **1** and **2** indicates the ferromagnetic coupling for both the Cu_6^{12+} and Mn_6^{12+} hexagons. The field (B) dependences of the magnetization (M) in electron Bohr magneton (μ_B) per mole units for **1** and **2** at 1.8 K are shown in Figure 3. The magnetization of **1** and **2** increases with increasing field with an approximately linear relationship at $B < 0.5$ and 0.1 T, respectively, and reaches a plateau. The plateau values of ~6.5 and 29 μ_B for **1** and **2** are close to the saturation values of 7 and 31 μ_B expected (for $g = 2$) for the isolated $S = 3$ and $S = 15$ states as spin-aligned ground states, respectively. The magnetic saturation with higher fields for **2** is faster than that for **1**, as expected from

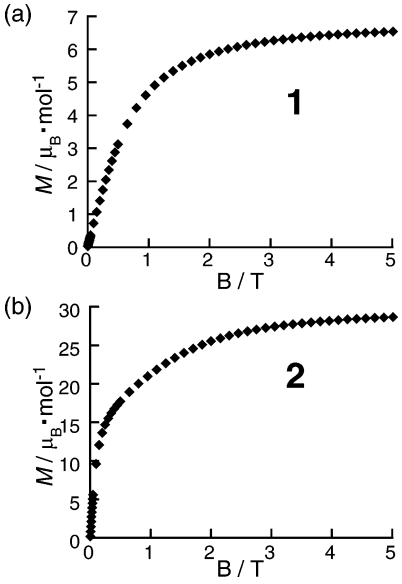

Figure 3. DC-field dependences of the magnetization (in μ_B) for **1** and **2** at 1.8 K.

the Brillouin function. The highest value of $\chi_m T$ for **1** is near the value (6.0 emu K mol^{-1}) expected for a spin-aligned $S = 3$ ground state, in which all six spins are parallel to each other, and the highest value for **2** is close to 120.0 emu K mol^{-1} for a spin-aligned $S = 15$ ground state. The drop of the $\chi_m T$ values below the cusp temperature for polycrystalline samples of **1** and **2** seems to be attributed to an increase of the contribution of the crystallines under the magnetic field along the hard direction to the magnetic susceptibility. Since second- and third-neighbor interactions between paramagnetic Cu^{2+} and Mn^{2+} ions with significantly long distance (more than 5 Å) within the Cu_6- and Mn_6-hexagons are weak enough to be assumed to be negligible, the Hamiltonian of the magnetic behavior of the Cu_6^{12+} and Mn_6^{12+} hexagons can be approximated by only first-neighbor interactions given by

$$H = -2J(\hat{S}_1\hat{S}_2 + \hat{S}_2\hat{S}_3 + \hat{S}_3\hat{S}_4 + \hat{S}_4\hat{S}_5 + \hat{S}_5\hat{S}_6 + \hat{S}_6\hat{S}_1) \quad (1)$$

where J refers to the isotropic magnetic exchange interactions for first-neighbor atoms of the approximately equilateral Cu_6^{12+} and Mn_6^{12+} hexagons according to the numbering scheme (Figure 1b), $\hat{S}_m$ and $\hat{S}_n$ are the spin angular momentum operators in units of $h/2\pi$ with the vector sum $S_{mn} = S_m + S_n$. The eigenvalues of the operators $(\hat{S}_m)^2$, $(\hat{S}_n)^2$, and $(\hat{S}_{mn})^2$ are $S_m(S_m + 1)$, $S_n(S_n+1)$, and $S_{mn}(S_{mn} + 1)$, respectively. A convenient formula for the energies (E) of the spin states which result from exchange coupling in the Cu_6^{12+} or Mn_6^{12+} hexagon with six magnetically equivalent Cu^{2+} or Mn^{2+} ions, developed by Van Vleck, is

$$E(S') = -J\{S'(S'+1) - 6S_i(S_i + 1)\} \quad (2)$$

where S' can take the values allowed by the vector summation rule and S_i is the total spin of atom i. Since the number of states (W) with a given S' is given by

$$W(S') = \Omega(S') - \Omega(S'+1) \quad (3)$$

where $\Omega(S')$ is the coefficient of $x^{S'}$ in the expansion of $(x^S$

(16) (a) Yamase, T.; Botar, B.; Ishikawa, E.; Fukaya, K. *Chem. Lett*. **2001**, 56. (b) Botar, B.; Yamase, T.; Ishikawa, E. *Inorg. Chem. Commun*. **2000**, *4*, 551. (c) Mialane, P.; Marrot, J.; Rivière, E.; Nebout, J.; Hervé, G. *Inorg. Chem*. **2001**, *40*, 44. (d) Robert, F.; Leyrie, M.; Hervé, G. *Acta Crystallogr*. **1982**, *B38*, 358. (e) Kortz, U.; Al-Kassem, N. K.; Savelieff, M. G.; Al Kadi, N. A.; Sadakane, M. *Inorg. Chem*. **2001**, *40*, 4742. (f) Bösing, M.; Nöh, A.; Koose, I.; Krebs, B. *J. Am. Chem. Soc*. **1998**, *120*, 7252. (g) Sazani, G.; Dickman, M. H.; Pope, M. T. *Inorg. Chem*. **2000**, *39*, 939.

$+ x^{S-1} + ... + x^{-S})^n$, χ_m can be evaluated according to the formula

$$\chi_m = (N\mu_B{}^2 g^2/3kT)\{\sum W(S')S'(S'+1)(2S'+1)\exp(-E(S')/kT\}/\{\sum W(S')(2S'+1)\exp(-E(S')/kT\} \quad (4)$$

where N is the Avogadro number, g the g factor, and k is the Boltzmann constant.[17] In eq 4, all the molecular-state g factors are assumed to be equal to the local g factors. When the low-lying states taken as the energy origin for **1** and **2** are $S = 3$ and 15 respectively, the expression of χ_m for **1** is

$$\chi_m = (2N\mu_B{}^2 g^2/kT)\{14 + 9\exp(-5x) + 25\exp(-3x)\}/\{7 + 5\exp(-6x) + 27\exp(-5x) + 25\exp(-3x)\} \quad \text{with } x = 2J/kT \quad (5)$$

and that for **2** is

$$\chi_m = (5N\mu_B{}^2 g^2/kT)\{126\exp(-119x) + 950\exp(-117x) + 3220\exp(-114x) + 7308\exp(-110x) + 12\,782\exp(-105x) + 18\,382\exp(-99x) + 22\,680\exp(-92x) + 24\,480\exp(-84x) + 23\,256\exp(-75x) + 19\,404\exp(-65x) + 14\,168\exp(-54x) + 9100\exp(-42x) + 4914\exp(-29x) + 2030\exp(-15x) + 496\}/\{111\exp(-120x) + 945\exp(-119x) + 2375\exp(-117x) + 4025\exp(-114x) + 5081\exp(-110x) + 6391\exp(-105x) + 6565\exp(-99x) + 6075\exp(-92x) + 5100\exp(-84x) + 3816\exp(-75x) + 2646\exp(-65x) + 1610\exp(-54x) + 875\exp(-42x) + 405\exp(-29x) + 145\exp(-15x) + 31\} \quad \text{with } x = 2J/kT \quad (6)$$

The best-fitting parameters obtained from a simulation of the χ_m versus T curve above the cusp temperature are $J/hc = +10.8$ cm^{-1} ($J/k = +15.5$ K) and $g = 2.06$ with the agreement factors, $R_\chi = [\sum\{(\chi_m)_{calcd} - (\chi_m)_{obsd}\}^2/\sum\{(\chi_m)_{obsd}\}^2] = 2.9 \times 10^{-4}$ and $R_{\chi T} = [\sum\{(\chi_m T)_{calcd} - (\chi_m T)_{obsd}\}^2/\sum\{(\chi_m T)_{obsd}\}^2] = 7.9 \times 10^{-3}$ for **1** and $J/hc = +0.14$ cm^{-1} ($J/k = +0.20$ K) and $g = 2.00$ with $R_\chi = 1.0 \times 10^{-4}$ and $R_{\chi T} = 3.6 \times 10^{-4}$ for **2**. As shown in Figure 2, however, there is a clear deviation for the $\chi_m T$ versus T fitting of **1**, while the fitting for **2** is convincing. The analysis using eq 5 for **1** reproduces the $\chi_m T$ data at a higher temperature range (above 70 K) quite well but does not account for data at lower temperature range (below 20 K), as is again discussed below.

Figure 4a and b shows the 190 GHz and 9.1 GHz ESR spectra of the single crystal ($0.5 \times 0.5 \times 0.4$ mm^3) of **1** under the orientation of a magnetic field with the z direction

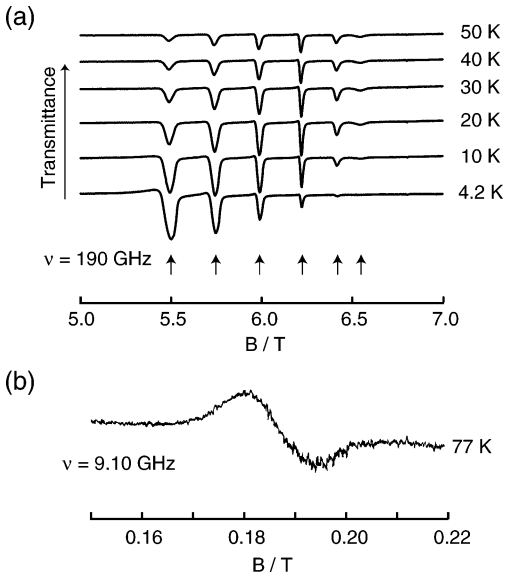

Figure 4. Temperature dependence of 190 GHz single-crystal ESR spectra (a) of **1** and 9.10 GHz single-crystal ESR spectrum (b) of **1** at 77 K. The ESR spectra were measured under the orientation of magnetic field along the c axis.

of the axial symmetric paramagnet (along a Cu_6^{12+} hexagon's nearly 6-fold axis equal to the c axis). The 190 GHz ESR spectra of the single crystal of **1** revealed six spin-allowed transitions ($\Delta S_Z = \pm 1$) around 5.5, 5.75, 6.0, 6.25, 6.4, and 6.6 T (with stronger intensity at lower fields at 4.2 K) which could be assigned to $|M_S\rangle = |-3\rangle \rightarrow |-2\rangle$, $|-2\rangle \rightarrow |-1\rangle$, $|-1\rangle \rightarrow |0\rangle$, $|0\rangle \rightarrow |+1\rangle$, $|+1\rangle \rightarrow |+2\rangle$, and $|+2\rangle \rightarrow |+3\rangle$ transitions for the $S = 3$ ground state, respectively. Although all the six separations between pairs of neighboring lines are not exactly the same (especially at $B \geq 6.4$ T) because of the contribution of the higher-order terms of the anisotropy to the transitions, nearly equal separations (0.245 T) between two neighboring lines at lower than 6.3 T should be equal to $2|D|/g\mu_B$, where D is the zero-field (fine-structure) energy separation between $S_z = 0$ and $S_z = \pm 1$ for $S = 3$. The negative sign on D was deduced from the observation (Figure 4a) that the lowest field line around 5 T was weakened at high temperature (for example, the strongest for the $|0\rangle \rightarrow |+1\rangle$ transition was around 6.25 T at $T \geq 30$ K). With the g value (2.22) obtained around 6.12 T on the 190G Hz ESR spectrum (Figure 4a), $D = -0.127$ cm^{-1}(-0.182 K) is obtained. The X-band (9.10 GHz) ESR spectrum of the single crystal of **1** at 77 K under the orientation of magnetic field along the c axis showed a singlet absorption observed at 0.186 T (Figure 4b), which is likely to be assigned to be the $|+2\rangle \rightarrow |+1\rangle$ transitions for both the ground state $S = 3$ and the excited state $S = 2$. Figure 5 shows the zero-field splitting and the ESR transitions under the Zeeman splitting with the orientation of magnetic field along the c axis for the $S = 3$ ground state of **1**. Since it is apparent that the energy levels resulting from the zero-field splitting for the lowest-lying $S = 3$ state will be distributed over a significant range at lower temperature (at $T < 20$ K), four energy levels ($S_z = \pm 3$, ± 2, ± 1, 0) of the $S = 3$ ground state in the Hamiltonian for **1**, given by inclusion of the D value, were taken into consideration in an effort to understand the low-temperature

(17) Boča, R. Theoretical foundations of molecular magnetism. In *Current Methods in Inorganic Chemistry Vol. 1*; Elsevier Science; Amsterdam, 1999.

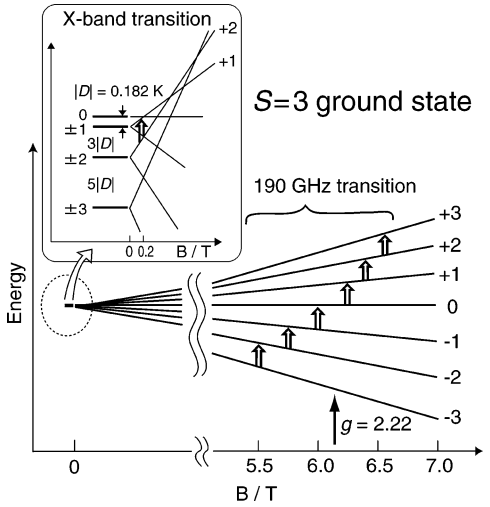

Figure 5. ESR transitions expected under the orientation of magnetic field along the *c* axis and zero-field splitting in the $S = 3$ ground state for **1**. White arrows indicate the expected 9.1 and 190 GHz ESR absorptions

deviation on the $\chi_m T$ versus T fitting (Figure 2a and eq 5). When $S_z = \pm 2$ is taken as the energy origin for $S = 3$, instead of eq 5, an alternative expression (eq 7) of χ_m at a low-temperature range above the cusp temperature for **1** is derived from eq 5

$$\chi_m = (2N\mu_B{}^2g^2/kT)\{4 + \exp(-3|D|/kT = -0.549/T) + 9\exp(5|D|/kT = 0.915/T) + 9\exp(-5x) + 25\exp(-3x)\}/\{2 + \exp(-4|D|/kT = -0.732/T) + 2\exp(-3|D|/kT = -0.549/T) + 2\exp(5|D|/kT = 0.915/T) + 5\exp(-6x) + 27\exp(-5x) + 25\exp(-3x)\} \text{ with } x = 2J/kT \quad (7)$$

The $\chi_m T$ data below 20 K (up to the cusp temperature of 7 K) could be reproduced well with eq 7: the resultant values are $J/hc = +9.34$ cm^{-1} ($J/k = +13.4$ K) and $g = 2.00$ with $R_{\chi T} = 7.4 \times 10^{-6}$. This accounts for the zero-field splitting (DS_z^2) in the $S = 3$ ground state at low temperature. Nevertheless, eq 7 did not explain the $\chi_m T$ data in the whole temperature range of 7−300 K ($J/hc = +18.0$ cm^{-1} ($J/k = +25.9$ K) and $g = 1.99$ with $R_{\chi T} = 3.9 \times 10^{-3}$), while the data above 70 K were in excellent fit of the $\chi_m T$ *versus* T curve achieved by eq 5 to provide $J/hc = +8.82$ cm^{-1} ($J/k = +12.7$ K) and $g = 2.27$ with $R_{\chi T} = 2.7 \times 10^{-5}$. Figure 6 shows the fitting of the $\chi_m T$ data for **1** at the lower temperature range of 7−20 K and at the higher temperature range of 70−300 K using eqs 7 and 5, respectively. Thus, the best fitting parameters obtained from the simulation of the $\chi_m T$ versus T curve above 70 K using eq 5 are employed for the magnetic behavior characteristic of the ferromagnetic interaction for **1**. Figure 7 shows that the energy separation between the ground state and the excited states is evaluated by substituting the coupling constants J (12.7 K for **1** (Figure 6b) and 0.20 K for **2** (Figure 2b) obtained by the fitting of the $\chi_m T$ data) back into eq 2. In Figure 7, the degeneracies of some of the states (calculated by eq 4) are also indicated. The large deviation (Figure 2) on fitting the $\chi_m T$ data for **1** in the low-temperature range using eq 5 in contrast to that (using eq 6) of **2** is probably associated with large $|D|$ value

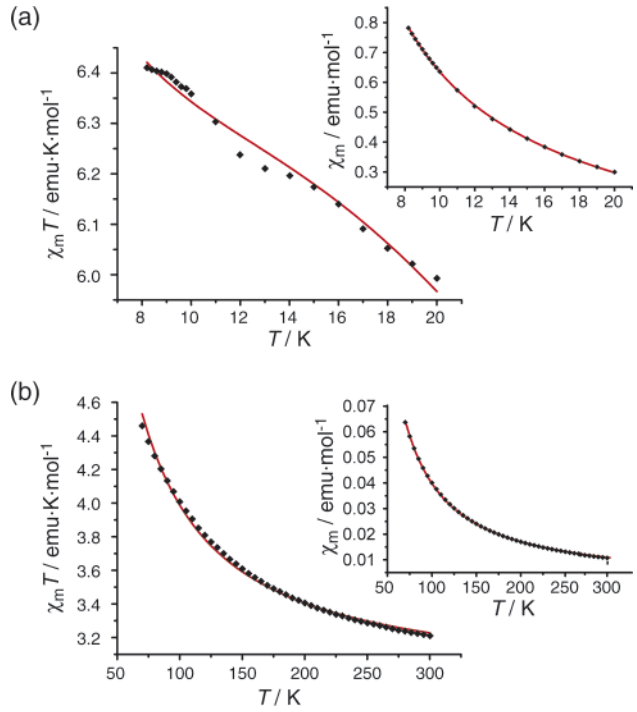

Figure 6. Fittings of the data below 20 K (a) using an alternative model (eq 7) which accounts for the zero-field splitting in the $S = 3$ ground state and the data above 70 K (b) using eq 5 for **1**. Red lines represent the calculated curves of χ_m vs T and $\chi_m T$ vs T curves above the cusp temperature using best fitting parameters for the data at 0.10 T (in the text).

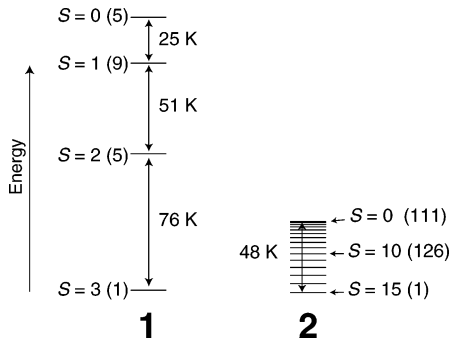

Figure 7. Zero-field energy splittings between magnetic states for **1** and **2**. The number in parentheses indicates the degeneracies of some of the magnetic spin states.

for **1**. The drop in the $\chi_m T$ values below the cusp temperature for polycrystallines of **1** and **2** (Figure 2) may be avoided by using single crystals, which enables us to measure the χ_m values under the magnetic field along the easy axis to reasonably fit the $\chi_m T$ data in the whole temperature range.

Conclusions

We have prepared and structurally characterized the first ferromagnetic D_{3d}-symmetric polyoxotungstates, $[(CuCl)_6(AsW_9O_{33})_2]^{12-}$ and $[(MnCl)_6(SbW_9O_{33})_2]^{12-}$ which contain Cu_6^{12+} and Mn_6^{12+} hexagons, respectively. The complexes, as *n*-$BuNH_3^+$ salts, indicate that *n*-$BuNH_3^+$ could be replaced by semiconducting or superconducting organic cations and that the resultant salts would be a good model for the understanding of the hybrid magnetic and conducting properties of the molecular interaction between the conducting electrons and the Cu_6^{12+}- or Mn_6^{12+}-hexagon spin moieties

in the lattice, as well as in the design of polyoxometalates-based molecular magnets. Furthermore, as is discussed in another paper, other D_{3d} Cu_6^{12+} and Mn_6^{12+} compounds with the same geometry, $(n\text{-}BuNH_3)_{12}[(CuCl)_6(SbW_9O_{33})_2]\cdot 6H_2O$ (with a first-neighbor Cu···Cu distance of 2.938(1) Å, Sb···Sb distance of 4.813(2) Å, and Cu−O−Cu angle of 94.9(3)−95.5(3)°) and $(n\text{-}BuNH_3)_{12}[(MnCl)_6(AsW_9O_{33})_2]\cdot 6H_2O$ (with a Mn···Mn distance of 3.228(2) Å, As···As distance of 5.408(2) Å, and Mn−O−Mn angle of 98.8(2)−99.0(2)°) are ferromagnetic (with $J/hc = +3.9$ cm^{-1} ($J/k = +5.6$ K) and $g = 2.49$) and antiferromagnetic (with $J/hc = -0.07$ cm^{-1} ($J/k = -0.09$ K) and $g = 1.88$), respectively. Also, an observable hysteresis loop on magnetization below 1.5 K with a pulsed field ($\sim 10^3$ T/s) for **1** involves the quantum tunneling of the adiabatic magnetization jump at level-crossing fields in addition to the thermal relaxation between $S_Z = \pm 3$ and $S_Z = \pm 2$. The D_{3d}-symmetric Cu_6^{12+} and Mn_6^{12+} hexagons imposed by polyoxotungstates are not only a simple model for the exchange-interaction study of molecular magnets but also provide a molecular design for novel magnetic devices.

Acknowledgment. This work was supported by Grants-in-Aid for Scientific Research 14204067 and 17002006 from the Ministry of Education, Science, Sports, and CREST of JST.

Supporting Information Available: Crystallographic data for **1** and **2** in CIF format. This material is available free of charge via the Internet at http://pubs.acs.org.

IC060666F